RSC Advances

ROYAL SOCIETY OF CHEMISTRY

www.rsc.org/advances

Multi-mode Photocatalytic Degradation and Photocatalytic Hydrogen Evolution of Honeycomb-like Three-dimensionally Ordered Macroporous Composite Ag/ZrO_2

Jingjing Zhang[a,b] Li Li[a,b,c*] Shuang Wang[a] Tingting Huang[a] Yuting Hao[b] Yunying Qi[b]

[a]College of Materials Science and Engineering, Qiqihar University, Qiqihar 161006, PR China

[b]College of Chemistry and Chemical Engineering, Qiqihar University, Qiqihar 161006, PR China

[c]College of Heilongjiang Province Key Laboratory of Fine Chemicals, Qiqihar University, Qiqihar 161006

Abstract: Three-dimensionally ordered macroporous composite (3DOM) Ag/ZrO_2 was prepared by using polystyrene (PS) colloidal spheres as the template and combined with the one-step method of vacuum impregnation. The composition, crystalline structure, morphology and surface physicochemical properties were characterized by ICP-AES, XRD, UV–vis/DRS, XPS, SEM and N_2 adsorption–desorption measurements. The results showed that the crystal type of 3DOM Ag/ZrO_2 was mainly tetragonal ZrO_2 phase, and Ag was present in the form of metallic silver, which had resulted in strong absorption in the visible region due to the effect of surface plasmon absorption (SPA). At the same time, the composite presented the three-dimensionally ordered macroporous structure well reproducing PS crystal template, whose Honeycomb-like structure was arranged in order, permeable and open, and the holes were closely connected with each other. The photocatalytic activity of 3DOM Ag/ZrO_2 was investigated by using Congo red as the model molecule. Compared with ZrO_2, P25 and Ag/ZrO_2, 3DOM Ag/ZrO_2 had the best photocatalytic activity under multi-modes including UV, visible light, simulated solar light and microwave-assisted irradiation. Moreover, the 3DOM Ag/ZrO_2 composite showed well effect on the degradation of different types of organic pollutants under UV light. Meanwhile, during the study of photocatalytic hydrogen production, the hydrogen yield of the 3DOM Ag/ZrO_2 composite was 18 times than that of commercial P25, which also showed excellent photocatalytic activity.

Keywords: Methanol vacuum impregnation method; Polystyrene; Three-dimensionally ordered macroporous materials; Ag/ZrO_2; Multi-mode photocatalysis; Photocatalytic hydrogen evolution

*Corresponding author
E-mail addresses: qqhrlili@126.com, qqhrll@163.com (L. Li).

Introduction

It is well known that the advantage of solar energy is enormous and inexhaustible, which is unmatched by other energy sources to a certain extent. Therefore, the study of the photocatalytic technology using solar energy has been taken people's attention[1-3]. On the current research, as an advanced technology, photocatalytic technology has broad potential applications in many areas, such as anti-bacteria, water treatment, air purification, hydrogen production from water and so on[4-6]. While hydrogen has become an ideal energy at present, in the case of igniting hydrogen, coal, and gasoline with the same weight, hydrogen can generate most energy, moreover, the main products are water, no ash and waste gas, and which will not pollute the environment. Therefore the photocatalytic hydrogen evolution is becoming many scientists' research hotspot[7-9].

The study of photocatalytic technology can't be separated with photocatalytic materials. At present, the materials used in photocatalysis are mainly semiconductor materials, such as TiO_2, ZnO and ZrO_2, etc, as the main body of the catalyst[10-12]. Among them, ZrO_2 is the only one which has both acidic and basic, and it's also the only metallic oxide which has oxidizability and reducibility. Since ZrO_2 is a kind of p-type semiconductor[13], it is easy to produce oxygen holes, as the carrier of the catalyst, which can produce interaction with active components. Therefore, it has more excellent performance than those catalysts supported by other materials. However, as a single semiconductor, Zirconia has high carrier recombination rate and low quantum efficiency; these faults limit its practical application in some degree. In view of this, at present, most of the researches are focused on the modification of ZrO_2 monomer by doping, compounding and other means to improve its photocatalytic activity[14]. About relevant literature of ZrO_2, the majority of ZrO_2 usually was complexed with TiO_2, such as, Polisetti et.al had synthesized TiO_2/ZrO_2 and carried out the degradation experiments on Alizarin Cyanine Green (ACG), but the experiments were proved that as-composite had no visible light activity[15]. Yu et.al had synthesized $Ti_{1-x}Zr_xO_2$ solid solutions by the citric acid complexing method, and the solid solutions exhibited higher photocatalytic activity than pure anatase TiO_2 for the degradation of acetone in air[16]. Sajid et al. had proposed that the deposited or doped metal in semiconductor may improve electron−hole separation and promote the interfacial electron transfer process, attributed to high Schottky barriers at the metal−semiconductor contact region and noble metal acting as electron traps, which can enhance the efficiency of the photocatalyst[17]. Wang et al. had prepared CdS/ZrO_2 by using the microwave-assisted hydrothermal, and studied the photocatalytic activity of CdS/ZrO_2 with different proportions, whose results showed that the photocatalytic effect of 30% CdS/ZrO_2 was the best[18]. Sasikala et al. proposed a catalyst including ZrO_2, TiO_2 and CdS, which showed higher photocatalytic activity for hydrogen production, moreover, the cocatalyst

adding 11.5% Pd into the TiO_2-CdS-ZrO_2 increased the lifetime of the light carrier, so enhanced its photocatalytic activity[19].

In addition, it is obvious to all that the studies were done on optimizing the morphology of composite materials and the activity of catalyst were improved by changing the morphology[20-22]. Three-dimensionally ordered macroporous materials (3DOM) have been one of the main research directions in the field of porous materials in recent years. Since three-dimensionally ordered macroporous materials not only have the characteristics of general porous material, but also include such traits as transparent space, arranged in neat and orderly, meanwhile, whose pore size is distributed uniformly, which shows good application prospect in many fields[23-27]. 3DOM both has characteristics of ordered macroporous structure and solid material, thereby, which has potential utilization value in physics and chemistry. Usually, the framework of 3DOM material may be composed of either single-component or multi-component, and has the good compatibility, which is easily to construct the novel functional materials that possess both specific composition and macroporous structure with cycles ordered characteristic; moreover, whose uniform pore size is adjustable, and tunnels arrange in orderly. Compared with other samples synthesized by conventional methods, the unique pore structure of the 3DOM material is very beneficial for the substances getting into the hole from all directions, which can reduce the diffusion resistance of material to some extent, providing higher efficiency diffusion of material. Among the traditional method of preparing three-dimensionally ordered macroporous materials, colloidal crystal template method is more practical. Jiao et al. had synthesized 3DOM TiO_2-supported CeO_2 photocatalyst by the colloidal crystal template method, under the action of heterojunction and the slow light effect of photonic crystal (3DOM structure), the composite material exhibited high catalytic activity for the photocatalytic reduction under simulated solar irradiation[29]. Arandiyan et al. had synthesized Pt/3DOM$Ce_{0.6}Zr_{0.3}Y_{0.1}O_2$ and 3DOM $Ce_{0.6}Zr_{0.3}Y_{0.1}O_2$ by the colloidal crystal template method, under the action of unique 3DOM structure and strong interaction between Pt nanoparticles, and as-synthesized 3DOM Pt/$Ce_{0.6}Zr_{0.3}Y_{0.1}O_2$ showed good low temperature reduction, and high catalytic performance for methane combustion[29].

Based on the above works and our existing research, our research group has carried out a series of research works on three-dimensionally ordered macroporous materials prepared by different kinds of composites, and some better results were obtained[30-32]. We have found that a variety of multi-layer, open 3DOM composite materials can be synthesized by polystyrene (PS) colloidal spheres template. After the composites prepared to form an excellent 3DOM material, of which the photocatalytic activity can be effectively improved to some extent. Accordingly, in this paper, on the one hand, hope to introduce three-dimensionally ordered macroporous structure into the synthesis of Ag/ZrO_2 composite by using the PS colloidal

crystal template method, and improve the photocatalytic activity of the composite by utilizing the open and permeable porous structure; On the other hand, using n-butoxypolyethylene zirconium as the precursor, self-assembling it with silver by taking advantage of the one-step method of vacuum impregnation, enhance light absorption by surface plasmon absorption (SPA) effect of Ag, and broaden the application range of ZrO_2 to improve the activity of 3DOM Ag/ZrO_2 nanocomposite, moreover, about which the study on its activity is from two aspects including photocatalytic degradation and photocatalytic hydrogen evolution.

1. Experimental

1.1. Materials

N-butoxypolyethylene zirconium ($C_{16}H_{36}O_4Zr$) was purchased from Shanghai Chunhe Biotechnology Co. Ltd., and the triblock poly(ethyl-ene oxide)-block-poly(propylene oxide)-block-poly(ethylene oxide) copolymer (P123) ($EO_{20}PO_{70}EO_{20}$, Mw = 5800) was purchased from Energy Chemical Company. NaOH, $K_2S_2O_8$ and isopropanol were purchased from Kaitong Chemical Reagent Co. Ltd., Tianjin, China. Degussa P25 (an efficient and industrial photocatalyst), styrene, p-benzoquinone (BQ), methanol (MA), disodium ethylenediamine tetraacetic acid (EDTA-2Na), congo red (CR), rhodamine B (RhB), crystal violet (CV), malachite green (MG) and phenol (Ph) were purchased from Guangfu Testmart, China; All other reagents were analytical reagent. Water used in all experiments was doubly distilled water.

1.2 Synthesis of Ag/ZrO_2

First, P123 was dissolved in isopropanol, then added n-butoxypolyethylene zirconium quickly under stirring conditions, after stirring well, added $AgNO_3$ solution with Ag and Zr molar ratio was 1:50. Treating the product at 200 ℃ for 2 h after forming Ag/ZrO_2 gel, as-obtained sample was vacuum dried and calcined in a muffle furnace at 500 ℃ for 7 h after grinding, and washed several times with ethanol and distilled water, marked as Ag/ZrO_2. Under the same experimental condition, the sample without adding $AgNO_3$ was marked as ZrO_2.

1.3. Synthesis of 3DOM Ag/ZrO_2

PS colloidal spheres synthesized by an emulsifier-free emulsion polymerization method[31] were added in methanol solution, stirred about 30 min at a constant speed, and then filtered it. $AgNO_3$ solution and n-butoxypolyethylene zirconium added in 10 mL isopropanol solution with Ag and Zr molar ratio was 1:50, added in treated PS colloidal spheres after mixing, stirred for 1 hour. Vacuum impregnation for 12 h, and then leached it. The product was calcined in a muffle furnace at 500 ℃ for 7 h, marked as 3DOM Ag/ZrO_2.

1.4. Characterization of photocatalysts

The phase and composition of the as-prepared samples were detected by Bruker-AXS

(D8) X-ray diffractometer (XRD) studies using an X-ray diffractometer with Cu Kα as X-ray radiation under 60 kV and 80 mA and with the 2θ ranging from 20º to 80º; and the ICP-AES was carried on an Agilent Technologies 7500ce inductively coupled plasma atomic emission spectrum. The optical properties of the samples were analyzed by UV–vis diffuse reflectance spectroscopy (DRS) using a UV–vis spectrophotometer (TU-1901) and equipped with a diffuse reflectance spectra over a wavelength range of 200–800 nm. The chemical composition analysis of the sample surfaces was made by X-ray photoelectron spectra (XPS) using an ESCALAB 250 Xi spectrometer with Al Kα radiation at 300 W, vacuum degree was 1×10^{-6} Pa. The morphologies and microstructures of the as-prepared samples were investigated by scanning electronmicroscope (SEM) (Hitachi S-4300), working voltage was 5 kV. The specific surface areas of the samples were measured by a Brunauer−Emmett−Teller specific surface area instrument (Beishide Instrumentation Technologies (Beijing) Ltd., Model 3H-2000PS2) with nitrogen adsorption at 77 K.

1.5. Photocatalytic degradation studies

The photocatalytic activities of 3DOM Ag/ZrO_2 composite were evaluated by photocatalytic degradation of crystal violet under multi-modes including UV, visible light, microwave-assisted and simulated solar light irradiation. The experimental reaction devices of a part of multi-mode light catalytic reaction are homemade, and the UV light source is 125 W high pressure mercury lamp (Built-in type, the maximum emission at 313.2 nm); the visible light was obtained from a 400 W Xe lamp (Built-in type, the main emission lines greater than 410 nm; the inner sleeve was made of No. 11 glass to filter out ultraviolet from the Xe lamp); A microwave discharge electrodeless lamp (MDEL, built-in type, UV emission wavelength mainly located at 280 nm) was used in the microwave-assisted test, the power was 15 W and the shape was an U model. The output power of the microwave was about 600 W[33]; Simulated sunlight source was carried out by using a 1000 W Xe-lamp (External type, Shanghai bilon Instruments Co., Ltd; the emission spectrum is close to the full spectrum; we carried out different experiments to check that O_3 could not be produced during the photocatalytic reaction process to discard the participation of the oxidizing agent in the decomposition of the dye). Congo red (CR) was used as a model dye. Process of photocatalytic reaction:

(1) UV light mode: Prior to irradiation, 0.15 g photocatalyst was suspended in 90 mL of CR (50 $mg\cdot L^{-1}$) solution by ultrasound *ca.*10 min, and then the suspensions were magnetically stirred for 30 min in the dark to ensure the adsorption/desorption equilibrium between CR and photocatalyst powders. The photocatalytic experiment was carried out in the photocatalytic reaction device. The high pressure mercury lamp was placed into a jacketed quartz tube. The quartz tube was soaked into the solution which was continuously magnetically stirred, and the

suspensions were kept at constant temperature by circulating water through the jacket during the entire process. At given time intervals, 3 mL of suspension was sampled and centrifuged to remove the photocatalyst particles. Then, the absorption spectrum of the centrifugated solution was recorded using a TU-1901 UV–vis spectrophotometer (China). The change of CR concentration was determined by monitoring the optical intensity of absorption spectra at 499 nm. Meanwhile, the absorbance values of RhB, CV, MG and Ph under similar photocatalytic conditions were measured at theirself λ_{max}.

(2) Visible light mode: 0.30 g photocatalyst was suspended in 220 mL of CR (50 $mg \cdot L^{-1}$), and the follow steps of experiment is the same as above except lamp source is 400 W Xe lamp.

(3) Microwave-assisted mode: 500 mL of CR (50 $mg \cdot L^{-1}$) solution and 0.50 g photocatalyst were taken in a microwave reactor and stirred for 30 min in the dark to ensure the adsorption/desorption equilibrium between CR and photocatalyst powders. The microwave reactor employed for the degradation of CR was purchased from Yuhua Instrument limited company of China. It consists of a cylindrical glass reactor (capacity 600 mL) with a 600 mm long water reflux condenser, connected through a communication pipe. The microwave discharge electrodeless lamp (MDEL) was placed into the reaction solution and about 2/3 parts of MDEL was dipped into reaction solution. Three silicone tubes were connected to the equipment, which could let water in and out and let air out through the hole on the microwave reactor. Air was bubbled into the solution through a sintered glass filter, fixed at the bottom of the reactor, not only for passing oxygen but also for mixing the catalyst and the solution. At given time intervals, 3 mL of suspension was sampled and centrifuged to remove the photocatalyst particles. Then, the absorption spectrum of the centrifugated solution was recorded using a TU-1901 UV–vis spectrophotometer (China).

(4) Simulated solar light mode: During the process of the simulated solar light irradiation, 90 mL of CR (50 $mg \cdot L^{-1}$) solution and 0.15 g photocatalyst were taken in a quartz photo-reactor and stirred for 30 min in the dark to ensure the adsorption/desorption equilibrium between CR and photocatalyst powders. The reactor was placed 8.5 cm away from the light source. The suspensions were kept at room temperature by circulating thermostated ethanol through the jacket. And the follow steps of experiment are the same as above UV light mode.

To infer the photocatalytic oxidation pathways of 3DOM Ag/ZrO_2, EDTA-2Na (1 mM), BQ (1 mM) and MA (1 mM) were selected as scavenger agents for holes (h^+), oxygen radical anion ($\cdot O_2^-$) and hydroxyl radicals ($\cdot OH$), respectively, for the photocatalytic degradation of CR over 3DOM Ag/ZrO_2 composite. The determination of concentration of CR during the photocatalytic reaction in the presence of EDTA-2Na, BQ or MA was also determined by

measuring the absorption of CR solution at 499 nm.

1.6 Photocatalytic hydrogen evolution test

Photocatalytic hydrogen evolution experiments were carried out in a reactor with a closed and connected vacuum circulatory system. 0.1 g photocatalyst was dispersed in 50 mL doubly distilled water, added $Na_2S·9H_2O$ as a sacrificial agent, after vacuum degassing, the test of photocatalytic hydrogen evolution started lighting under the condition of stirring. The light source was 300 W Xe lamp; high purity nitrogen being carrier gas, output pressure was 0.4~0.5 MPa, and working voltage and working current was about 20 mV and 50 mA, respectively. In the reaction process, the temperature of the reactor was kept at 5 ℃ by the circulating cooling water. Gas was collected after a certain irradiation, by using online gas chromatography to analyze the hydrogen production; the reaction was carried out for 8 h. The column is 5 Å molecular sieve column, and the detector is thermal conductivity detector (TCD). According to the peak area of the different reaction time, the production of hydrogen was calculated. And the catalytic activity of the photocatalyst was measured by the total hydrogen production of 8 h.

2. Results and discussion

2.1 ICP and XRD analysis

The loadings of Ag in the samples were determined using the ICP-AES technique, the results as shown in Table 1. According to the results of ICP-AES test, we can get two pieces of information. First, the low amounts of Ag actually present in the 3DOM Ag/ZrO_2 and Ag/ZrO_2. Second, the difference of synthesis method can affect Ag content in the composites. Compared with the Ag/ZrO_2 and 3DOM Ag/ZrO_2, Ag/ZrO_2 have fewer amount of Ag, attributed to that part Ag hadn't been formed and was washed away by ethanol and distilled water.

The crystal structure and crystallinity of the 3DOM Ag/ZrO_2, Ag/ZrO_2, ZrO_2 and Ag were studied by XRD detection, the results as shown in Fig. 1. From Fig. 1, pure ZrO_2 is tetragonal phase, and the diffraction peaks are located at 30.22º, 34.96º, 50.29º and 60.22º (PDF 50-1089)[34]. Pure Ag is cubic phase crystal structure, of which the main diffraction peak is 38.3º, 44.39º, 64.55º and 77.51º (PDF 04-7083). Fig. 1 appeared that the peaks of 3DOM Ag/ZrO_2 at 2θ values of 30.2º, 35.2º, 50.4º, 60.0º in the XRD patterns were indexed to the ZrO_2 tetragonal phase (011), (110), (112), (121) crystalline plane, respectively, which showed that the doping of Ag didn't cause the change of ZrO_2 crystal. In addition, the characteristic diffraction peaks of Ag were not observed in the XRD pattern of 3DOM Ag/ZrO_2. This may be due to the high dispersion of Ag on the surface of the composite[35]. Compared with that of pure ZrO_2 (a=b=3.6072 Å, c=5.1482 Å), it did not significantly change that the lattice parameters of 3DOM Ag/ZrO_2 (a=b=3.5983 Å, c=5.1555 Å), showing that Ag did not enter

into the ZrO_2 crystal lattice, therefore, Ag is more likely to be dispersed on the surface of ZrO_2 in the form of nanoparticles. Simultaneously, compared with ZrO_2, the lattice parameters of Ag/ZrO_2 decrease slightly, which may be due to the defect made by the temperature-programmed hydrothermal treatment during the synthesis process, so that the degree of crystallinity decreased[36]. From Fig. 1, it can also be seen, the diffraction peak of 3DOM Ag/ZrO_2 is sharper than that of ZrO_2, indicating that the crystallinity of 3DOM Ag/ZrO_2 is higher. According to the Scherrer formula[18], the grain sizes of the samples are shown in Table 1. From Table 1, the grain size of 3DOM Ag/ZrO_2 is significantly larger than that of Ag/ZrO_2, attributed to the different of synthesis methods, and 3DOM can effecte on the grain[37].

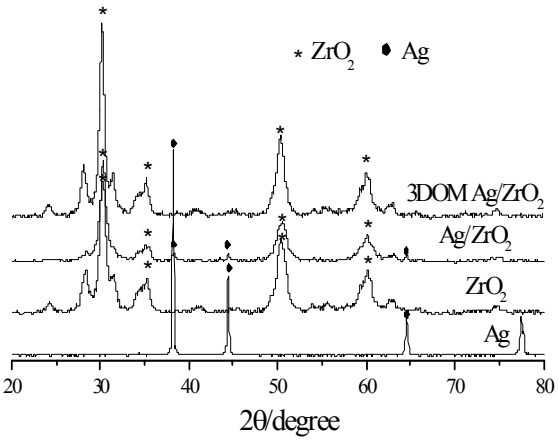

Fig. 1 XRD patterns of 3DOM Ag/ZrO_2, Ag/ZrO_2, ZrO_2 and Ag.

Table 1. Crystallite size(*D**), band-gap energy(*Eg*), BET surface areas (S_{BET}), average pore diameters (*D*), pore volumes (*Vtotal*), cell parametersand and ICP-AES data of 3DOM Ag/ZrO_2 and Ag/ZrO_2.

Sample	S_{BET} ($m^2 \cdot g^{-1}$)	*D* (nm)	*Vtotal* ($cm^3 \cdot g^{-1}$)	*D** (nm)	*Eg* (eV)	Crystal parameters		mole ratio of precursor n(Ag):n(Zr)	actual mole ratio n(Ag):n(Zr)
						a/Å	c/Å		
Ag/ZrO_2	54.9	15.3	0.210	10.6	3.51	3.6029	5.1450	1:50	1:57
3DOM Ag/ZrO_2	33.3	20.0	0.166	15.1	3.25	3.5983	5.1555	1:50	1:48

The Scherrer formula[18]: $D=K\lambda/B\cos\theta$ (K is Scherrer constant, *D* is the average thickness of the grains perpendicular to the plane direction (nm); *B* is the measured half-width of the diffraction peak sample, θ is diffraction angle; λ is the wavelength of X-rays).

2.2 XPS analysis

In order to study the chemical forms of the various elements on the surface of the composite, 3DOM Ag/ZrO_2 was analyzed by XPS, the results as shown in Fig. 2. It can be seen, the surface of 3DOM Ag/ZrO_2 mainly has three elemental species: Ag, Zr and O. According to Fig. 2(a), the binding energy of zirconium element on 3DOM Ag/ZrO_2

composite is 181.9 eV and 184.1 eV, respectively, corresponding to $Zr3d_{5/2}$ and $Zr3d_{3/2}$, and this element is ascribed to the Zr^{4+} oxidation state[38]. Fig. 2(b) is the binding energy of the silver element on the composite in the XPS spectra; the peaks at 368.0 eV and 374.0 eV are attributed to $Ag3d_{5/2}$ and $Ag3d_{3/2}$, respectively. Spin energy interval is 6.0 eV, indicating that Ag was present in the form of metallic silver[39,40]. In addition, Fig. 2(c) appears O1s peak at 529.9 eV and 531.2 eV, respectively, belonging to the lattice oxygen and the adsorbed oxygen in composite[41].

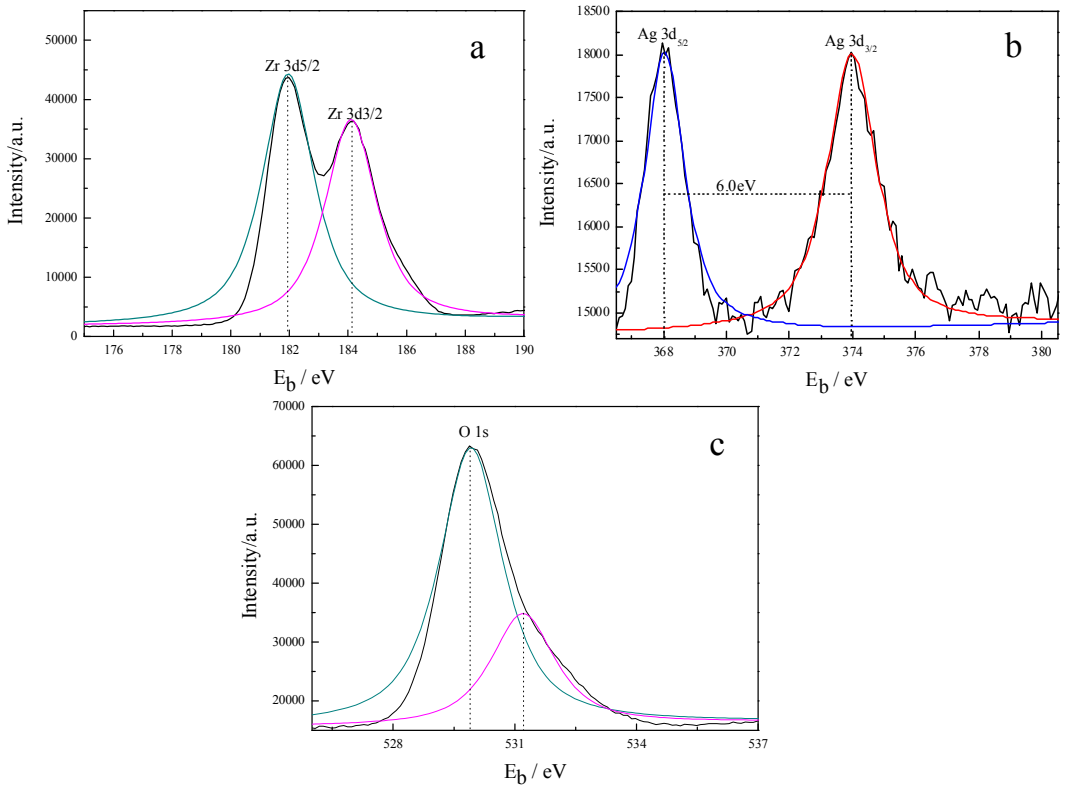

Fig. 2 XPS spectra of 3DOM Ag/ZrO_2, (a) Zr3d, (b) Ag3d and (c) O1s.

2.3 SEM analysis

To study the morphology and the size of the composites, SEM analysis was carried out on the polystyrene and 3DOM Ag/ZrO_2, the results as shown in Fig. 3. Among them, Fig. 3(a, c) is the SEM images of PS colloidal spheres under different magnifications. Fig. 3(a) shows the synthesized polystyrene colloidal spheres template has a highly ordered array, and the surface of PS colloidal spheres is smooth, whose size is relatively uniform and the average diameter is *ca.*300 nm. The PS colloidal spheres are arranged closely, and each polystyrene colloidal sphere is simultaneously exposed to the other six spheres, presenting like "honeycomb" hexagonal close-packed structure, attributed to the result of a relatively tight arrangement when the PS colloidal spheres are self-assembled[42]. Fig. 3(b, d) is the SEM images of the composite after calcination to remove the PS colloidal spheres. It can be observed from Fig. 3(b, d), the product presents three-dimensionally ordered macroporous

interconnection state, and the bottom of each large hole is composed of three small windows, meanwhile, holes are connected, open and transparent. This indicates that the product is well replicated the derived structure of the PS colloidal spheres template. However, due to the removal of the synthesis of PS colloidal spheres template is carried out by calcined treatment, if the control of temperature is not uniform at the time of calcination, there will be a small amount of PS colloidal spheres template not be completely removed, for example, the upper right part of the region can still be observed PS that colloidal spheres aren't fully calcined clean in Fig. 3(b). The above three-dimensionally ordered macroporous materials are arranged in order, whose sizes are uniform and *ca.* 210 nm. In addition, looking closely at illustrations and the enlarged view of partial region in the Fig. 3(b, d), it is not difficult to find, the pore walls of these ordered macroporous pores are closely packed with Ag/ZrO_2 nanocrystals. Compare with Fig. 3(a, c) and (b, d), it shows that the pore size of the 3DOM composite is smaller than the diameter of the PS template, due to the high temperature of the calcination process cause the shrinkage of the aperture[43].

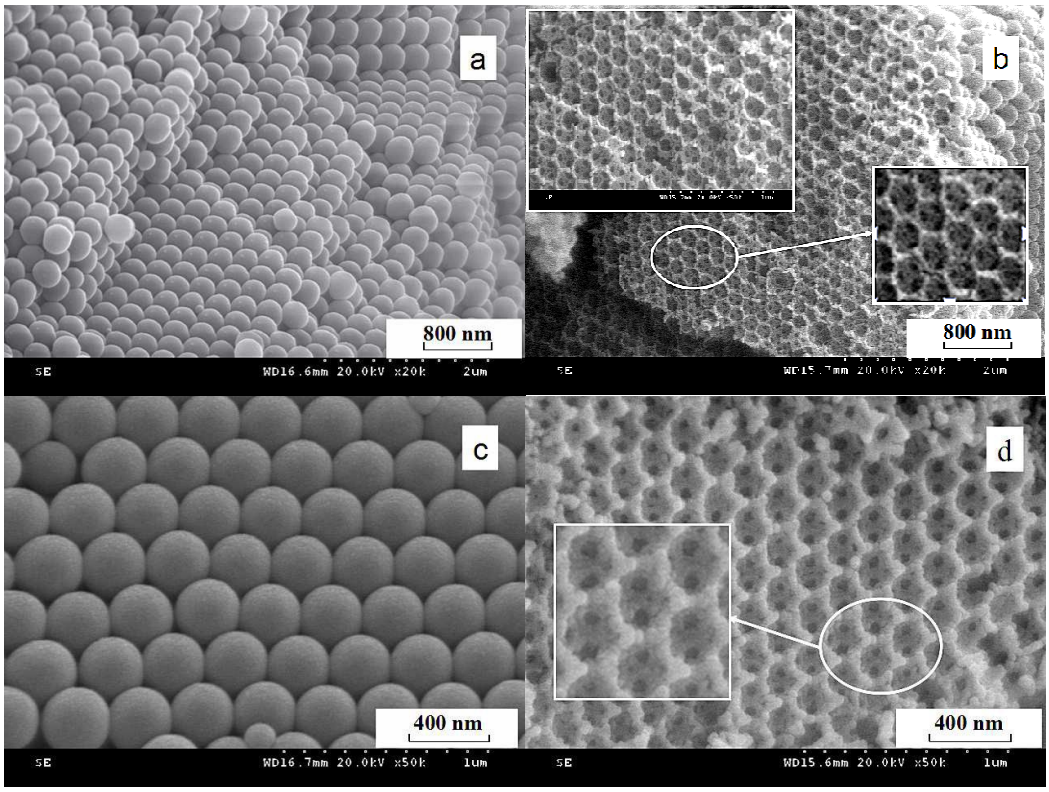

Fig. 3 SEM images of PS (a, c) and 3DOM Ag/ZrO_2 (b, d).

2.4. UV–vis/DRS analysis

The UV–vis diffuse reflectance spectra (UV–vis/DRS) were carried out to investigate the optical absorption of 3DOM Ag/ZrO_2, the results as shown in Fig. 4 and Table 1. It can be seen from Fig. 4, compared to ZrO_2, the absorption peaks of 3DOM Ag/ZrO_2 and Ag/ZrO_2 have some red-shifts, and both are red-shifted to the visible region. This result can be

attributed to the surface plasmon absorption (SPA) of Ag nanoparticles in the composites[44]. Additionally, as shown in Fig. 4, the absorption of 3DOM Ag/ZrO_2 sample prepared by self-assembly of PS colloidal spheres template in the range of 250–800 nm is significantly higher than that of Ag/ZrO_2. On the one hand, which is attributed to the doping amounts of Ag in the two composites have slight differences due to the different synthesis methods, leading to the different light absorption properties of Ag/ZrO_2 and 3DOM Ag/ZrO_2 composites; on the other hand, also due to the special morphology of 3DOM material producing multiple scattering of light, so as to increase the contact time between light and the composite material[45]. At the time of UV–vis/DRS detection, the open and transparent macroporous structure of 3DOM Ag/ZrO_2 is easier to make the light be reflected by the Ag in the deep layer, and produces a stronger absorption response.

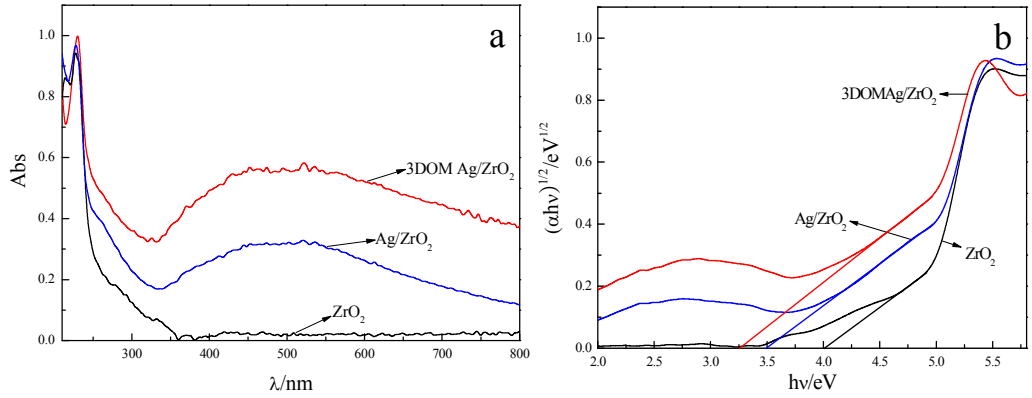

Fig. 4 UV–vis/DRS spectra (a) and Kubelka-Munk energy curve plots of ZrO_2, Ag/ZrO_2 and 3DOM Ag/ZrO_2 (b).

At the same time, the bandgap energy values (Eg) of ZrO_2, Ag/ZrO_2 and 3DOM Ag/ZrO_2 were calculated by Kubelka-Munk plot (Fig. 4(b)), and the band gap (Eg) of the semiconductors can be obtained from eq 1[46]:

$$\alpha h\nu = A(h\nu\text{-}Eg)^{n/2} \quad (1)$$

In the aforementioned formula, α, ν and A are absorption coefficient, light frequency and proportionality constant, respectively. The n can be determined by the type of optical transition of a semiconductor (i.e., n = 1 for direct transition and n = 4 for indirect transition), the results as seen Table 1. Since the Eg is smaller, the excited required wavelength is greater under illumination, so the electron is more easily to transition, and the quantity is bigger. According to Table 1, the lower Eg value of 3DOM Ag/ZrO_2 can affect on its light-absorbing properties, therefore, 3DOM Ag/ZrO_2 composite will have a higher photocatalytic activity.

2.5 N_2 adsorption–desorption analysis

To evaluate surface physicochemical properties of as-synthesized composites, N_2 adsorption–desorption measurements were measured for 3DOM Ag/ZrO_2, and compared with

the prepared composite Ag/ZrO_2, the results as shown in Fig. 5 and Table 1. According to Fig. 5, the N_2 adsorption–desorption isotherms of 3DOM Ag/ZrO_2 and Ag/ZrO_2 emerge IV type adsorption curve type[47], which is a typical mesoporous structure adsorption isotherm. The biggest characteristic of this type is the hysteresis loop of 3DOM Ag/ZrO_2 belonging to H3 type[31], and the isotherm type and its hysteresis loop is caused by the aggregation of the capillary and the aggregation of the particles in the structure. In addition, the hysteresis loop of Ag/ZrO_2 belongs to H1 type[48], and the adsorption and desorption of the hysteresis loop are parallel, corresponding to round tubular structure opening at both ends[49]. The mesoporous structure of 3DOM Ag/ZrO_2 should be attributed to the large-hole wall of the composite material. As shown in Fig. 5, the BET surface areas of Ag/ZrO_2 is larger than that of 3DOM Ag/ZrO_2, which should be due to add templating agent P123 in the synthesis process of Ag/ZrO_2, resulting in the specific surface area increase[50]. It can be seen from the illustration of Fig. 5, the pore size of 3DOM Ag/ZrO_2 is more uniform than that of Ag/ZrO_2 in the BJH pore size distributions curves of two kinds of composite materials, and this should be attributed to the 3DOM synthesis method used in this paper. Due to using the methanol vacuum impregnation method during the synthesis, the precursor is uniformly filled in between the polystyrene microspheres; resulting in internal structure of 3DOM Ag/ZrO_2 is uniform and orderly.

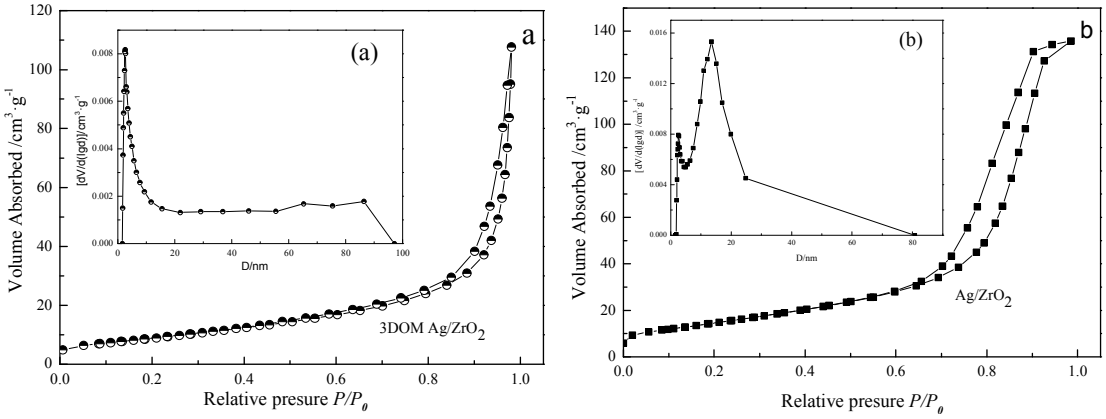

Fig. 5 N_2 adsorption–desorption isotherms of 3DOM Ag/ZrO_2 (a) and Ag/ZrO_2 (b) (Illustrations are BJH pore size distribution curves).

2.6 Photocatalytic activity for the degradation of dyes

In order to investigate the photocatalytic performance of 3DOM Ag/ZrO_2 composite, a series of multi-mode photocatalysis experiments were carried out under UV light, visible light, simulation sunlight and microwave-assisted irradiation etc, the results as shown in Fig. 6. In addition, to study a series of photocatalytic properties of 3DOM Ag/ZrO_2, we use commercial P25 as the comparing objects, whose purpose is more objectively to evaluate the photocatalytic effect of 3DOM Ag/ZrO_2 in this paper[51,52]. According to Fig. 6, the

photocatalytic activity of 3DOM Ag/ZrO_2 is significantly higher than the other samples under UV light irradiation conditions. In the illustration of Fig. 6(a), $-ln(C_t/C_0)$ (C_0 refers to the initial concentration of the reaction solution after the completion of the adsorption experiments; C_t is the concentration of the reaction solution at the time of t) has a linear relationship with reaction time *t*, which shows that the degradation of dye Congo red follows pseudo first-order kinetics. After calculation, the apparent reaction rate constants of the degradation of congo red by direct photocatalysis, P25, ZrO_2, Ag/ZrO_2 and 3DOM Ag/ZrO_2 are 0.00030, 0.00847, 0.00041, 0.00299 and 0.01489 min^{-1}, respectively, therefore, under UV light irradiation conditions, the order of catalytic activity is 3DOM Ag/ZrO_2>P25>Ag/ZrO_2>ZrO_2>direct photocatalysis. Furthermore, the photocatalyst 3DOM Ag/ZrO_2 was used for the degradation of different organic contaminants, including congo red (CR), rhodamine B (RhB), crystal violet (CV), malachite green (MG) and phenol (Ph) under similar conditions of UV irradiation as shown in Fig. 6(b). It can be seen from Fig. 6(b), the degradation effect of 3DOM Ag/ZrO_2 on different types of dyes and phenol is better under UV light, showing 3DOM Ag/ZrO_2 has extensive for different types of organic matter degradation. Fig. 6(c) presents the results of photocatalytic degradation CR under other different modes including visible light, simulated solar light and microwave-assisted irradiation. As shown in Fig. 6c, each mode described above the degradation effect is not as obvious as UV light. But compared with direct photocatalysis, the degradation rate is obviously improved, futhermore, the degradation rate under microwave-assisted irradiation is faster than other two modes due to microwave effect promote the reaction process[53,54]. Moreover, Fig. 6(c) also exhibits that the photocatalytic activity of 3DOM Ag/ZrO_2 is significantly higher than that of the other photocatalysts under microwave-assisted irradiation, and 3DOM Ag/ZrO_2 has a relatively high activity in these experimental conditions, may be due to the incorporation of Ag make 3DOM Ag/ZrO_2 red shift and enhance light absorption, which helps to improve the photocatalytic activity; At the same time, the transparent hole structure of 3D ordered macroporous materials can effectively reduce the diffusion resistance of the material, which make the dyes and other reactant molecules more easily reach the active center. Simultaneously, the catalyst has a highly ordered macroporous structure, which can enhance its periodicity, moreover, the contact surface between the dye molecules and the catalyst is increased, so more reactive sites can be further enhanced its activity.

At the same time, the active groups in the system of 3DOM Ag/ZrO_2 during the process of photocatalysis were investigated, in which, p-benzoquinone (BQ), the methanol (MA) and EDTA-2Na were added as scavenger agents to capture superoxide radicals ($\cdot O_2^-$), hydroxyl ($\cdot OH$) and holes (h^+), respectively, and compared with the experiment without capture agents (Fig. 6(d)). The results showed, the addition of three trapping agents had a certain inhibition

effect on the degradation of congo red[55,32]. It showed that three capture agents have a certain degree of capture on the active substance of the photocatalytic reaction, suggesting the active groups of 3DOM Ag/ZrO_2 are mainly superoxide radicals ($\cdot O_2^-$), hydroxyl ($\cdot OH$) and holes (h^+) in photocatalytic process.

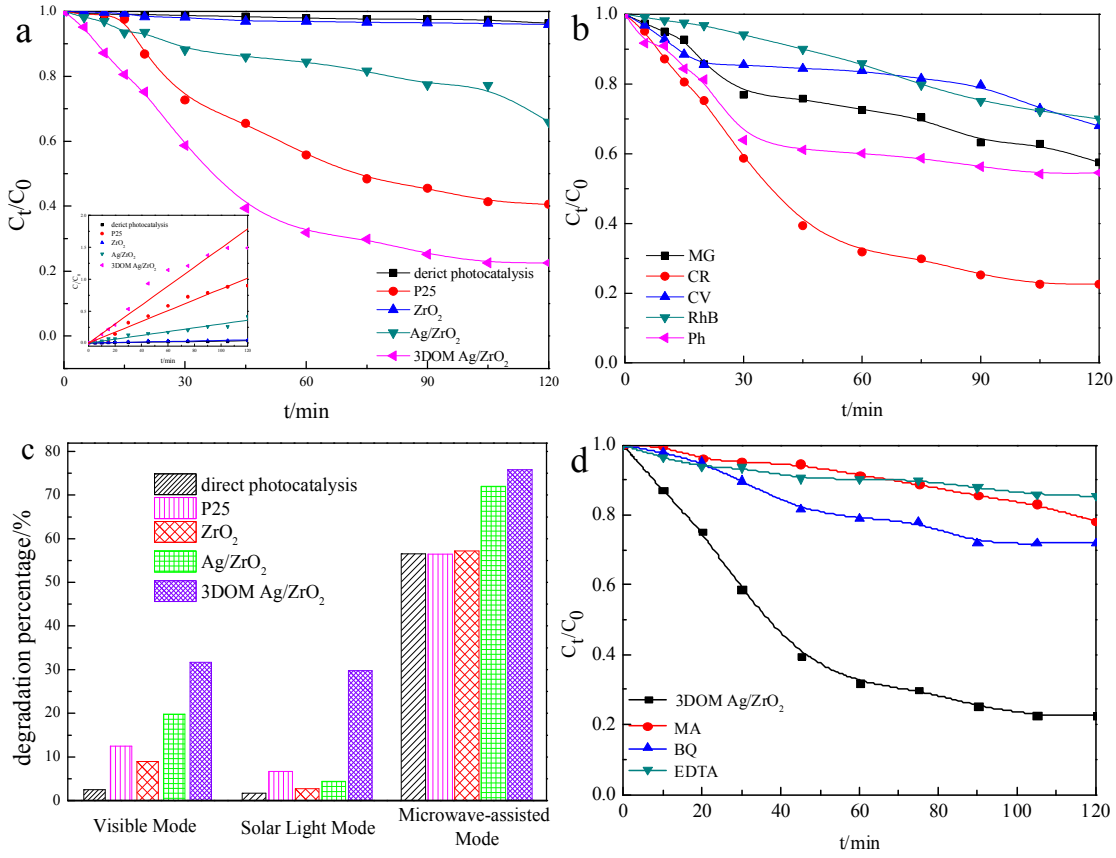

Fig. 6 a. UV photocatalytic degradation CR using different photocatalysts and Kinetics curves (inset)(a); b. UV photocatalytic degradation different organic pollutants using 3DOM Ag/ZrO_2; c. photocatalytic degradation of CR using different photocatalysts under multi-modes including visible light(t=180 min), microwave-assisted (t=90min) and simulated solar light irradiation (t=240 min); d. UV photocatalytic degradation CR capture test using 3DOM Ag/ZrO_2.

2.7 Photocatalytic hydrogen evolution

In order to investigate the activity of 3DOM Ag/ZrO_2 composite in photocatalytic hydrogen evolution reaction, the experiments were carried out for 8 h in this article, the results as shown in Fig. 7. Fig. 7 shows that hydrogen production efficiencies of ZrO_2 and P25 are lower, mainly due to the light electrons and holes of semiconductor monomer quickly compound and occurr hydrogen reverse reaction and so on[18]. The activity of photocatalytic hydrogen evolution of 3DOM Ag/ZrO_2 was much higher than that of Ag/ZrO_2 and two monomers, attributed to certain amount of Ag nanoparticles doping in the composite materials, which increased the absorption of light and enhanced the photocatalytic activity.

In addition, the result that the hydrogen production efficiency of 3DOM Ag/ZrO_2 was higher than that of the Ag/ZrO_2 sample by simple preparing, showing that the three-dimensionally ordered macroporous structure is the key to improve the hydrogen production activity. By introducing the three-dimensionally ordered structures, of which open inner surface favors the reduction reaction, and the open pores can help output produced H_2 timely and reduce the reverse reaction.

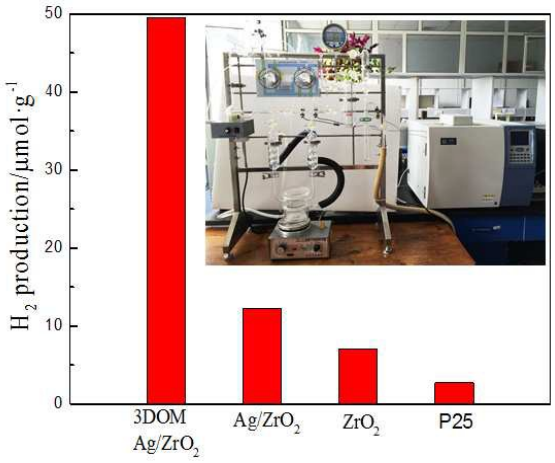

Fig. 7 Hydrogen production amount of 3DOM Ag/ZrO_2, Ag/ZrO_2, ZrO_2 and P25.

2.8 Possible photocatalytic reaction mechanism

Based on the above results and related experimental data, this article speculates 3DOM Ag/ZrO_2 possible photocatalytic mechanism, as shown in Fig. 8. It can be seen from Fig. 8, on the one hand, the visible response of 3DOM Ag/ZrO_2 is enhanced due to Ag surface plasmon resonance effect, which generates more photogenerated carriers, and improves the photocatalytic activity; on the other hand, after the p-type semiconductor ZrO_2 loads Ag nanoparticles, due to the work function of Ag (4.26 eV[56]) is greater than that of ZrO_2 (3.5 eV[15]), the Schottky barrier is formed between them[17]. ZrO_2 is excited to produce electrons and holes in the photocatalytic process, and electrons are gathered in the contact surfaces of Ag and ZrO_2 due to the Schottky barrier function. Meanwhile, noble metal Ag can act as electron traps and promote electron-hole separation, increase electron transfer between interfaces, thereby enhancing the photocatalyst efficiency; According to the formula of $E_{(CB)}=\chi-Ee-0.5Eg$ and $E_{(VB)}=E_{(CB)}+Eg$[57], determining the redox potential of the conduction band and valence band of the composite material are -0.22 and 3.03 eV, respectively, the result is not only satisfy the condition of photocatalytic degradation of organic matter, while the potentialof the valence band of samples is more negative than hydrogen, so the sample also has photocatalytic hydrogen evolution activity. And then the photogenerated electrons reacting with O_2 adsorbed on the catalyst surface generates superoxide radicals, at the same time, the holes and the water generate hydroxyl radicals, superoxide radicals and hydroxyl radicals can

degrade organic pollutants completely, even mineralize to CO_2 and H_2O and so on. In this paper, the prepared Ag/ZrO_2 belongs to three-dimensionally ordered macroporous material with multilayered and open, of which the open pore structure makes the organic contaminants be sufficiently contracted with the photocatalyst, and improves the photocatalytic reaction efficiency further. At the same time, the position of the conduction band of the 3DOM Ag/ZrO_2 is negative to the hydrogen electrode reaction potential (0 eV), which can satisfy the requirements of hydrogen evolution reaction, that is, conduction band electron may reduce water into hydrogen. Since the as-synthesized composite 3DOM Ag/ZrO_2 can simultaneously satisfy the above conditions of degradation and hydrogen production, therefore, 3DOM Ag/ZrO_2 may have both photocatalytic degradation and photocatalytic hydrogen evolution activity. In addition, introducing the three-dimensionally ordered macroporous structure also can help output produced H_2 timely, and improve the photocatalytic reaction efficiency further.

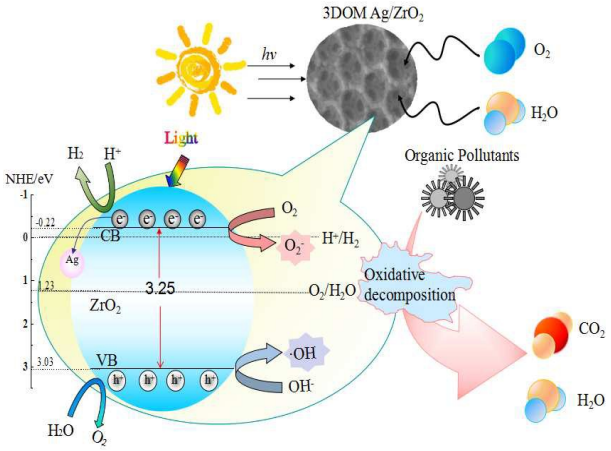

Fig. 8 Possible photocatalytic reaction mechanism of 3DOM Ag/ZrO_2.

Conclusion

Using PS colloidal spheres as self-assembling template, via methanol vacuum impregnation method and postprocessing calcination, 3DOM Ag/ZrO_2 composite was prepared. The as-composite not only has well crystal structure, but also Ag existing as metallic silver can enhance the absorption of the composite in the visible region due to the SPA effect. At the same time, the composite has uniform, transparent and similar "honeycomb" macroporous structure by processing the colloidal crystal template, the hole wall is piled up by nanoparticles. The photocatalytic activity of 3DOM Ag/ZrO_2 was higher than that of direct photolysis, P25, ZrO_2 and Ag/ZrO_2 in the multi-mode photocatalytic degradation of Congo red, moreover, which has a certain effect on the degradation of many organic pollutants. Meanwhile, 3DOM Ag/ZrO_2 also has good ability on photocatalytic hydrogen evolution, showing that the synergistic effect after Ag and ZrO_2 complexed, and the

three-dimensionally ordered macroporous structure introduced into the synthesis of composite will help improve its photocatalytic activity.

Acknowledgements

This study are supported by the National Natural Science Foundation of China (21376126), Natural Science Foundation of Heilongjiang Province, China (B201106), Scientific Research of Heilongjiang Province Educaton Department (12511592,12541888), Government of Heilongjiang Province Postdoctoral Grants, China (LBH-Z11108), Open Project of Green Chemical Technology Key Laboratory of Heilongjiang Province College, China (2013 year), Postdoctoral Researchers in Heilongjiang Province of China Research Initiation Grant Project (LBH-Q13172), Innovation Project of Qiqihar University Graduate Education (YJSCX2015-ZD03), College Students' Innovative Entrepreneurial Training Program Funded Projects of Qiqihar University (201510221077) and Qiqihar University in 2015 College Students Academic Innovation Team Funded Projects.

Reference

1 Y. Zhong, Z. X. Wang, R. F. Zhang, F. Bai, H. M. Wu, R. Haddad, and H. Y. Fan. *ACS Nano*, 2014, **8**, 827−833.

2 Y. Yang, G. Z. Wang, Q. Deng, and H. J. Zhao. *ACS Appl. Mater. Inter.*, 2014, **6**, 3008−3015.

3 J. Y. Xiong, Z. Li, J. Chen, S. Q. Zhang, L. Z. Wang, and S. X. Dou. *ACS Appl. Mater. Interfaces*, 2014, **6**, 15716–15725.

4 J. Liu, Y. Liu, N. Y. Liu, Y. Z. Han, X. Zhang, H. Huang, Y. Lifshitz, S. T. Lee, J. Zhong, and Z. H. Kang. *Science,* 2015, **347**, 970−974.

5 Z. G. Zou, , J. H. Ye, K. Sayama, and H. Arakawa. *Nature*, 2001, **414**, 625−627.

6 W. Y. Teoh, J. A. Scott, and R. Amal. *J. Phys. Chem. Lett*., 2012, **3**, 629–639.

7 Y. B. Wang, Y. S. Wang, and R. Xu. *J. Phys. Chem. C*, 2013, **117**, 783−790.

8 J. H. Yang, D. Wang, H. X. Han, and C. Li. *Acc. Chem. Res.*, 2013, **46**, 1900–1909.

9 J. Y. Zhang, Y. H. Wang, J. Zhang, Z. Lin, F. Huang, and J. G. Yu. *ACS Appl. Mater. Inter.*, 2013, **5**, 1031−1037.

10 A. Pearson, S. K. Bhargava, and V. Bansal. *Langmuir*, 2011, **27**, 9245–9252.

11 P. Gomathisankar, K. Hachisuka, H. Katsumata, T. S. Kunihiro Funasaka, and S. Kaneco. *ACS Sustain. Chem. Eng.*, 2013, **1**, 982−988.

12 W. W. Xia, C. Mei, X. G. Zeng, G. K. Fan, J. F. Lu, X. D. Meng, and X. S. Shen. *ACS Appl. Mater. Inter*, 2015, **7**, 11824−11832.

13 K. Samson, M. Ś liwa, R. P. Socha, K. Gora-Marek, D. Mucha, D. Rutkowska-Zbik, J-F.Paul, M. Ruggiero-Mikołajczyk, R. Grabowski, and J. Słoczynski. *ACS Catal.*, 2014, **4**, 3730−3741.

14 Y. L. Yu, P. Zhang, Y. J. Kuang, Y. H. Ding, J. H. Yao, J. J. Xu, and Y. A. Cao. J. *Phys. Chem.*

C, 2014, **118**, 20982–20988.

15 S. Polisetti, P. A. Deshpande, and G. Madras. *Ind. Eng. Chem. Res.*, 2011, **50**, 12915−12924.

16 J. C. Yu, J. Lin, and R. W. M. Kwok. *J. Phys. Chem*. B, 1998, **102**, 5094−5098.

17 S. I. Mogal, V. G. Gandhi, M. Mishra, S. Tripathi, T. Shripathi, P. A. Joshi, and D. O. Shah. *Ind. Eng. Chem. Res.*, 2014, **53**, 5749–5758.

18 L. Li, L. L. Wang, W. Z. Zhang, X. L. Zhang, X. Chen, X. Dong. *J Nanopart Res*, 2014, **16**, 2753.

19 R. Sasikala, A. R. Shirole, S. R. Bharadwaj. *J Colloid Interf Sci*, 2013, **409**, 135–140.

20 N. Roy, Y. Park, Y. Sohn, K. T. Leung, and D. Pradhan. *Mater. Inter*, 2014, **6**, 16498−16507.

21 F. Li, Z. Y. Wang, and A. Stein. *Angew. Chem. Int. Ed*., 2007, **46**, 1885–1888.

22 S. J. Ding, X. Yin, X. J. Lu, Y. M. Wang, F. Q. Huang, and D. Y. Wan. *ACS Appl. Mater. Inter.*, 2012, **4**, 306−311.

23 O. D. Velev, T. A. Jede, R. F. Lobo, and A. M. Lenhoff. *Nature*, 1997, **389**, 447−448.

24 J. E. G. J. Wijnhoven, W. L. Vos. *Science*, 1998, **281**, 802−804.

25 A. A. Zakhidov, R. H. Baughman, Z. Iqbal, C. X. Cui, I. Khayrullin, S. O. Dantas, J. Marti, and V. G. Ralchenko. *Science*, 1998, **282**, 897−899.

26 B. T. Holland, C. F. Blanford, and A. Stein. *Science*, 1998, **281**, 538−540.

27 R. C. Schroden, M. Al-Daous, S. Sokolov, B. J. Melde, J. C. Lytle, A. Stein, M. C. Carbajo, J. T. Fernández, and E. E. Rodríguez. *J. Mater. Chem.*, 2002, **12**, 3261−3267.

28 J. Q. Jiao, Y. C. Wei, Z. Zhao, J. Liu, J. M. Li, A. J. Duan, and G. Y. Jiang. *Ind. Eng. Chem. Res*., 2014, **53**, 17345−17354.

29 H. Arandiyan, H. X. Dai, K. M. Ji, H. Y. Sun, and J. H. Li. *ACS Catal*., 2015, **5**, 1781−1793.

30 L. Lu, L. Li, T. Y. Hu, W. Z. Zhang, X. D. Huang, and J. Q. Zhang. *Mol. Catal. A-Chem*, 2014, **394**, 283−294.

31 L. Li, X. D. Huang, T. Y. Hu, J. X. Wang, W. Z. Zhang, and J. Q. Zhang. *New. J. Chem*, 2014, **38**, 5293−5302.

32 L. Li, X. D. Huang, J. Q. Zhang, W. Z. Zhang, F. Y. Ma, and Z. X. Xiao. *J Colloid Interf Sci*, 2015, **443**, 13–22.

33 L. Li, Y. Ma, Y. Z. Cao, Y. Ji, and Y. H. Guo. *Acta Phys-Chim. Sin*., 2009, **25**, 1461–1466.

34 H. Lu, A. Khan, S. E. Pratsinis, and P. G. Smirniotis. *Energ Fuel*, 2009, **23**, 1093–1100.

35 H. Arandiyan, H. X. Dai, J. G. Deng, Y. Wang, H. Y. Sun, S. H. Xie, B. Y. Bai, Y. X. Liu, K. M. Ji, and J. H. Li. *J. Phys. Chem. C*, 2014, **118**, 14913−14928.

36 D. M. Chen, Z. H. Wang, T. Z. Ren, H. Ding, W. Q. Yao, R. L. Zong, and Y. F. Zhu. *J. Phys. Chem. C*, 2014, **118**, 15300–15307.

37 G. Chojnowski, R. Przenios, I. Sosnowska, M. Bukowski, H. Natter, R. Hempelmann, A. Fitch and V. Urban. *J. Phys. Chem. C*, 2007, **111**, 5599–5604.

38 J. S. Wang, Y. L. Yu, S. Li, L. M. Guo, E. J. Wang, and Y. A. Cao. *J. Phys. Chem. C*, 2013, **117**,

27120–27126.

39 R. C. Gamez, E. T. Castellana, and D. H. Russell. *Langmuir*, 2013, **29**, 6502–6507.

40 D. H. Yu, X. D. Yu, C. H. Wang, X. C. Liu, and Y. Xing. *ACS Appl. Mater. Inter*, 2012, **4**, 2781–2787.

41 R. Vaidya, R. J. Simonson, J. Cesarano III, D. Dimos, and G. P. López. *Langmuir*, 1996, **12**, 2830–2836.

42 W. A. Abdallah and S. D. Taylor. *J Phys Chem C*, 2008, **112**, 18963–18972.

43 G. I. N. Waterhouse, J. B. Metson, H. Idriss, and D. X. Sun. *Chem. Mater*., 2008, **20**, 1183–1190.

44 M. Anpo, T. Shima, S. Kodama, and Y. Kubokawa. *J. Phys. Chem.*, 1987, **91**, 4305–4310.

45 H. Xie, Y. Z. Li, S. F. Jin, J. J. Han, and X. J. Zhao. *J. Phys. Chem. C*, 2010, **114**, 9706–9712.

46 T. I. Draskovic, M. Z. Yu, and Y. Y. Wu. *Inorg. Chem.,* 2015, **54**, 5519-5526.

47 S. L. Zou and G. C. Schatz. *J Chem Phys.*, 2004, **121**, 12606.

48 X. H. Wang, Y. K. Zhang, C. Hao, F. Feng, H. B. Yin, and N. C. Si. *Ind. Eng. Chem. Res*., 2014, **53**, 6585−6592.

49 C. Larese, J. M. Campos-Martin, and J. L. G. Fierro. *Langmuir*, 2000, **16**, 10294–10300.

50 M. Davis, D. A. Ramirez, and L. J. Hope-Weeks. *ACS Appl. Mater. Inter*., 2013, **5**, 7786–7792.

51 H. G. Baldoví, S. Neaţu, A. Khan, A. M. Asiri, S. A. Kosa, and H. Garcia. *J. Phys. Chem. C*, 2015, **119**, 6819–6827.

52 H. Hirakawa, M. Katayama, Y. Shiraishi, H. Sakamoto, K. L. Wang, B. Ohtani, S. Ichikawa, S. Tanaka, and T. Hirai. *ACS Appl. Mater. Interfaces*, 2015, **7**, 3797–3806.

53 Y. Sakaguchi, A.V. Astashin, B. M. Tadjikov. *Chem. Phys. Lett*, 1997, **280**, 481–488.

54 J. Literák, P. Klán. J. Photochem. *Photobio. A: Chem*., 2000, **137**, 29–35.

55 K. S. W. Sing, D. H. Everett, R. A. W. Haul, L. Moscou, R. A. Pierotti, J. Rouquerol, and T. Siemieniewska. *Pure & App. Chem.*, 1985, **57**, 603–619.

56 D. D. Lin, H. Wu, R. Zhang, and W. Pan. *Chem. Mater.*, 2009, **21**, 3479–3484.

57 Y. Xu, and M. A. A. Schoonen. *Am. Mineral*, 2000, **85**, 543–556.

Graphical abstract

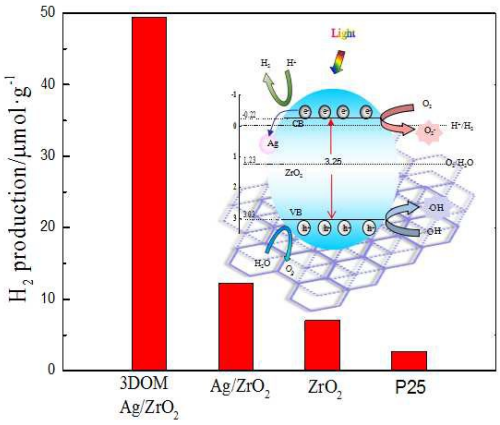

The Honeycomb-like three-dimensionally ordered macroporous composite 3DOM Ag/ZrO_2 was prepared by using polystyrene (PS) colloidal spheres as template and combined with the one-step method of vacuum impregnation, which has both good photocatalytic degradation under multi-modes and ability on photocatalytic hydrogen evolution.